

# Elongation dynamics of amyloid fibrils: a rugged energy landscape picture

Chiu Fan Lee\*

*Physics Department, Clarendon Laboratory, Oxford University, Oxford OX1 3PU, UK*

James Loken

*Physics Department, Denys Wilkinson Building, Oxford University, Oxford OX1 3RH, UK*

L  titia Jean and David J. Vaux

*Sir William Dunn School of Pathology, Oxford University, Oxford OX1 3RE, UK*

(Dated: November 13, 2018)

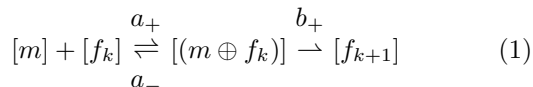
Protein amyloid fibrils are a form of linear protein aggregates that are implicated in many neurodegenerative diseases. Here, we study the dynamics of amyloid fibril elongation by performing Langevin dynamic simulations on a coarse-grained model of peptides. Our simulation results suggest that the elongation process is dominated by a series of local minimum due to frustration in monomer-fibril interactions. This rugged energy landscape picture indicates that the amount of recycling of monomers at the fibrils' ends before being fibrilized is substantially reduced in comparison to the conventional two-step elongation model. This picture, along with other predictions discussed, can be tested with current experimental techniques.

PACS numbers: 87.14.ef, 82.35.Pq, 83.10.Mj, 46.25.Cc

## I. INTRODUCTION

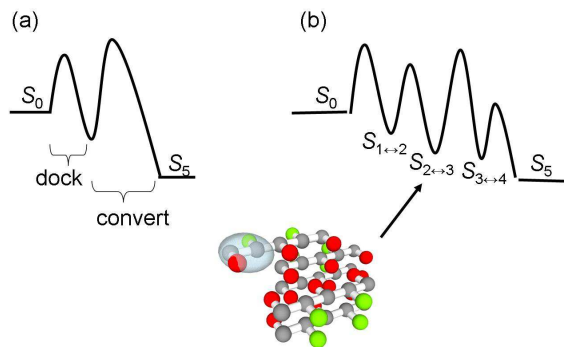
Amyloids are insoluble fibrous protein aggregations stabilized by a network of hydrogen bonds and hydrophobic interactions [1, 2, 3, 4]. They are intimately related to many neurodegenerative diseases such as Alzheimer's Disease, Parkinson's Disease and prion diseases [5]. Better characterization of the various properties of amyloid fibrils is therefore of high importance for the understanding of the associated pathogenesis. In this paper, we investigate the dynamics of elongation in fibril growth.

From the kinetic theory point of view, the elongation process is traditionally viewed as a diffusion-limited reaction coupled with high free-energy barrier crossing [6]. A more refined picture has also been proposed in [7, 8, 9, 10, 11, 12] where the elongation process is treated as a two-step dock-and-convert process (c.f. Fig. 1(a)). Namely, the elongation process follows the kinetics scheme:



where  $[m]$  denotes the monomer concentration,  $[f_k]$  the fibril concentration consisting of  $k$  monomers,  $[(m \oplus f_k)]$  denotes the intermediate state before a monomer can be converted into fibril, and  $a_+$ ,  $a_-$  and  $b_+$  are the corresponding rates. Experimentally, elongation rates for amyloid fibrils formed from various peptides have been measured (e.g., [10, 12, 13, 14]). In particular, A $\beta$  fibrils, which are implicated in the pathogenesis

of Alzheimer's disease [5], have an estimated conversion-limiting elongation rate of  $\sim 0.3 \mu\text{m}/\text{min}$  [14]. Given that each beta strand is about 0.5 nm in width, this elongation rate translates to be in the order of one monomer fibrilized per second, i.e.,  $b_+ \sim 1 \text{ s}^{-1}$ . Intuitively, the intermediate state  $(m \oplus f_k)$  corresponds to the initial state when the monomer first becomes bound to the fibril's end through hydrophobic interactions or/and a small number of hydrogen bonds. This suggests that at the initial binding, the energy gain,  $\Delta U$ , should amount to only a few



\*Corresponding author: C.Lee1@physics.ox.ac.uk

$k_B T$  [15]. If we estimate  $a_-$  by treating the undocking process as a diffusion-limited dissociation, then (see, e.g., ch. 8 in [16]):

$$a_- \sim \frac{3De^{\Delta U}}{r^2}, \quad (2)$$

where  $r$  is the distance between the two reactants, which is of the order of 1 nm. Taking the binding energy,  $\Delta U$  to be  $-3k_B T$ , say, and setting  $D$  to be  $10^{-10} \text{ m}^2\text{s}^{-1}$ , which is a typical diffusion constant for small proteins [16],  $a_-$  can be estimated to be about  $10^7 \text{ s}^{-1}$ . Since  $b_+ \sim 1 \text{ s}^{-1}$  and  $a_- \sim 10^7 \text{ s}^{-1}$ , the two-step model depicted in Eq. (1) suggests that almost  $10^7$  monomers would have been interacted with the fibril's end before one of them is converted [40] under the experimental condition investigated in [14].

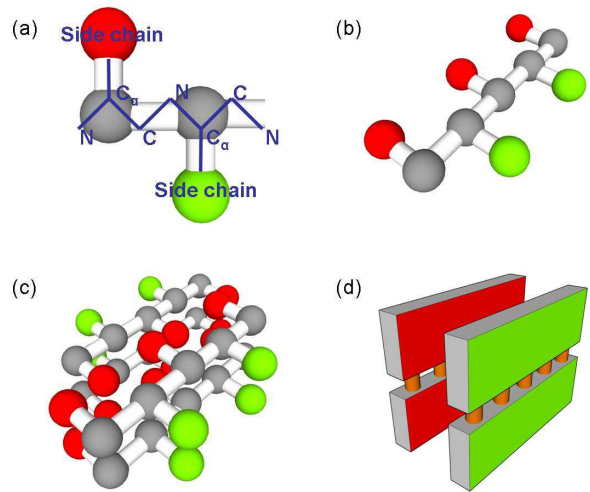
In this work, we demonstrate, with the help of coarse-grained molecular dynamics simulations, that the dynamics in the conversion step is dominated by a series of energy traps manifested by the frustrated monomer-fibril interactions, which would include i) the misalignment of the monomer with respect to the beta strands at the fibril's end; ii) frustrated hydrophobic interactions among the side chains; and iii) the competition to bind between multiple monomers at the same end of a growing fibril. In this picture, there is not a rate limiting step for the elongation process, but rather, each energy trap contributes to the final elongation rate observed. This scenario is akin to the random energy model investigated in glassy systems (e.g., see [17]). This rugged energy landscape picture predicts that monomers would spend a substantial amount of time at the fibril's end before conversion. As a result, the amount of recycling of the monomers at the fibrils' ends before one of them becomes fibrilized would be many orders of magnitude small than the value indicated by the two-step model depicted in Eq. 1. This dynamical picture is testable by, e.g., performing fibril elongation experiments with a small portion of monomers radioactively tagged [10, 12].

We will now present the details on the simulation method is presented in Section II. In Section III, we explain how the simulation results are analyzed. In Section IV, we discuss how our findings relate to the rugged energy picture introduced and present some implications of our model. We then end with a conclusion.

## II. SIMULATION DETAILS

Employing coarse-grained peptide models for the study of amyloids are abundant in the literature (e.g., [18, 19, 20, 21, 22, 23, 24, 25]), here we aim to use the simplest model to study amyloid fibril elongation. Specifically, we keep only two types of inter-peptide interactions: directional interactions provided by hydrogen bonds, and undirectional interactions given by hydrophobic interactions. The directional interactions dictate that fibrils can only grow linearly, and the undirectional interactions are

FIG. 2: Schematic pictures depicting the model adopted in this work. (a) Each amino acid is simplistically represented by two beads, the gray beads represent the peptide backbone of an amino acid and the coloured beads the side chains (red for hydrophobic and green for hydrophilic). We stress that the representation is only meant to be qualitative. (b) The five-amino-acid peptide employed in this work with alternating hydrophilic-hydrophobic side chains. The alternating pattern has been shown to promote amyloid fibril formation [33, 34, 35, 36, 37, 38]. (c) A segment of fibril consisting of four peptides in two layers of cross-beta sheets. (d) A cartoon depicting the four beta strands corresponding to (c). The green (red) face of the panel depicts the hydrophilic (hydrophobic) side.



indispensable in keeping the fibrils thermodynamically stable [26]. The directionality of the hydrogen bonds suggests that each amino acid has to be represented by at least two set of coordinates, one for its position and one for the direction of the side-chain. We therefore minimally employ two beads to represent each amino-acid (c.f. Fig. 2(a)). We stress that we do not attempt to devise a quantitatively correct representation of a peptide, but rather to use a toy model to study the elongation process.

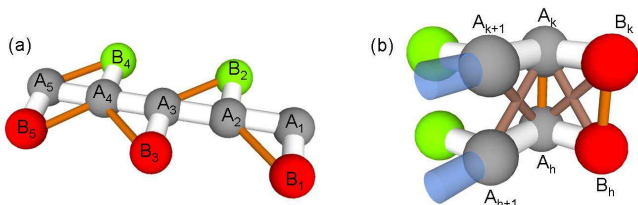
We will now describe the details of the model. For simplicity, there are only two types of interactions:

$$V(r, \kappa, \sigma, d) = \begin{cases} \frac{\kappa}{d^2}(r - \sigma)^2 - \kappa & , \quad |r - \sigma| < d \\ 0 & , \quad \text{otherwise} \end{cases} \quad (3)$$

$$W(r, \kappa, \sigma, d) = \begin{cases} \kappa \left[ \left(\frac{\sigma}{r}\right)^{12} - 2 \left(\frac{\sigma}{r}\right)^6 \right] & , \quad r < d \\ 0 & , \quad \text{otherwise} \end{cases} \quad (4)$$

Namely,  $V$  is a harmonic potential with a sharp cutoff at  $d$  (in units of nm) and  $W$  is the Lennard-Jones potential again with a cutoff at  $d$ ,  $\sigma$  (in units nm) denotes the minimum in the potential well and  $\kappa$  controls the depth of the potential well (in units of  $k_B T$ ). Note the dis-

FIG. 3: The bonded interactions for the model. (a) Besides the white bonds between the beads, the orange bonds are employed to fix the angle between the side-chains and the peptide backbone. Note that the side-chain at the end of the peptide,  $B_5$ , is bonded to  $A_4$  in order to maintain the angle  $B_5 - A_5 - A_4$ . (b) The six bonding interactions in the  $D$ -bond between beads  $A_k$  and  $A_h$ . If one of the  $A$  beads involved is at the end of the peptide, e.g.,  $A_h = A_5$ , then the cross-peptide  $A$ - $A$  bonds will be between  $A_k - A_5$ ,  $A_{k+1} - A_5$  and  $A_k - A_4$  instead.



continuities in the slopes of the potentials at the cutoffs. We believe that these discontinuities are unimportant in our Langevin simulations due to the greater magnitude of perturbation from thermal fluctuation.

The whole system is modeled by pairwise interactions consisting of a linear sum of a set of potentials  $V$  and  $W$ , which can be categorized into two classes: bonded interactions and non-bonded interactions.

### A. Bonded interactions

Bonded interactions refer to the bonds within a peptide in order to provide it with the structural constraints that mimic a peptide (c.f. Fig. 3). The parameters of the interactions are shown in Table I(a). For example, the total force acting on the bead  $A_1$  due to bonded interactions is:

$$\vec{\nabla}_{A_1} \left[ V(r_{A_1 A_2}, 40, 1/2, \infty) + V(r_{A_1 B_1}, 40, 1/2, \infty) + V(r_{A_1 A_3}, 10, 1, \infty) \right], \quad (5)$$

where  $\vec{\nabla}_{\alpha} \equiv \vec{\nabla}_{\mathbf{r}_{\alpha}}$  and  $r_{\alpha\beta} = |\mathbf{r}_{\alpha} - \mathbf{r}_{\beta}|$  with  $\mathbf{r}_{\alpha}$  referring to the position of the  $\alpha$  bead. The first term fixes the inter-amino-acid distance to be about 0.5 nm and the second term dictates that the distance between the peptide backbone and the side chain to be about 0.5 nm. The second term above gives longitudinal rigidity to the peptide.

TABLE I: (a) The parameters employed in the bonded interactions. The potential is of the form  $V$  with  $d = \infty$  and the values in the entries correspond to  $(\kappa, \sigma)$ . (b) The parameters for  $U$ -type non-bonded interactions. The potential is of the form  $W$  and the values in the entries correspond to  $(\kappa, \sigma, d)$ . (c) The parameters for  $D$ -type non-bonded interactions. The potential is of the form  $V$  and the values in the entries correspond to  $(\kappa, \sigma, d)$ . Note that these interaction potentials are only switched on when all six distances are within the cutoffs.

(a) Bonded interactions

	$A_1$	$A_2$	$A_3$	$B_1$
$A_1$	-	(40, 1/2)	(10, 1)	(40, 1/2)
$B_1$	(40, 1/2)	(40, 2 <sup>-1/2</sup> )	-	-

(b)  $U$ -type non-bonded interactions between every pair of beads not bonded

	$A_i$	$B_{j=\text{even}}$	$B_{j=\text{odd}}$
$A_i$	(5, 1/2, 1/2)	(5, 1/2, 1/2)	(5, 1/2, 1/2)
$B_{j=\text{even}}$	(5, 1/2, 1/2)	(5, 1/2, 1/2)	(5, 1/2, 1/2)
$B_{j=\text{odd}}$	(5, 1/2, 1/2)	(5, 1/2, 1/2)	(3/2, 1/2, 1)

(c)  $D$ -type non-bonded interactions between beads  $A_i$  and  $A_j$

	$A_i$	$B_j$	$A_{j+1}$
$A_i$	(4, 1/2, 1/10)	(4, 2 <sup>-1/2</sup> , 3/20)	(4, 2 <sup>-1/2</sup> , 3/20)
$B_j$	(4, 2 <sup>-1/2</sup> , 3/20)	(4, 1/2, 1/10)	-
$A_{j+1}$	(4, 2 <sup>-1/2</sup> , 3/20)	-	-

### B. Non-bonded interactions

Besides the bonded interactions, there are also non-bonded interactions between the beads. The first type is unidirectional and we call them  $U$ -type interactions.

#### 1. $U$ -type interactions

These interactions include steric constraints or attractive interactions (only between pairs of hydrophobic beads, i.e.,  $B_{i=\text{odd}}$ ) between every pair of beads, except for pairs already under bonded interactions. These effects are manifested by the the Lennard-Jones potential with different cutoffs,  $d$ :  $d = \sigma$  for the case of pure repulsion, and  $d > \sigma$  for the case of long range attraction with short range repulsion. The parameters employed in the simulations are shown in Table Ib. For instance, the interaction potential between two red beads,  $B_i$  and  $B_j$ , is  $V(r_{B_i B_j}, 1, 1/2, 1)$ .

## 2. *D*-type interactions

We use the term *D*-bonds to refer to the directional interactions between peptides. The *D*-bonds are meant to mimic the cross-beta sheet hydrogen bonds. We will model the directional elements by a sum of six harmonic potentials  $V$  (c.f. Fig. 3(b)). This way of modeling directionality in hydrogen bonding is akin to the works employing discrete molecular dynamics simulations to study amyloid formation in the literature [19]. Note that the potentials are only switched on when all six pairwise distances concerned are within their respective cutoffs. In other words, the total interaction potential for a *D*-type bond between  $A_i$  and  $A_j$  is:

$$\begin{aligned} & \theta \left[ V(r_{A_i A_j}, 5, 1/2, 1/10) + V(r_{A_i B_j}, 5, 2^{-1/2}, 3/20) \right. \\ & + V(r_{A_i A_{j+1}}, 5, 2^{-1/2}, 3/20) + V(r_{B_i A_j}, 5, 2^{-1/2}, 3/20) \\ & \left. + V(r_{B_i B_j}, 5, 1/2, 1/10) + V(r_{A_{i+1} A_j}, 5, 2^{-1/2}, 3/20) \right], \end{aligned}$$

where  $\theta = 1$  when all of the six distances are within their respective cutoffs, and  $\theta = 0$  otherwise.

### C. Simulation procedure

We performed Langevin dynamics simulations on our system. Namely, the position of the  $\alpha$  bead,  $\mathbf{r}_\alpha$ , follows the updating rule [29]:

$$\mathbf{r}_\alpha(t+\Delta t) = \mathbf{r}_\alpha(t) = \frac{1}{\gamma} \vec{\nabla}_\alpha U_{\text{total}}(\{\mathbf{r}\}) \Delta t + \sqrt{\frac{2k_B T}{\gamma}} \Delta t \vec{\eta}_\alpha, \quad (6)$$

where  $\vec{\eta}_\alpha$  represents Gaussian noise with zero mean and variance one in 3D,  $\gamma$  is the friction coefficient for each bead, and  $U_{\text{total}}$  is the sum of all pairwise interactions in the model. The relevant parameters are shown in Table II.

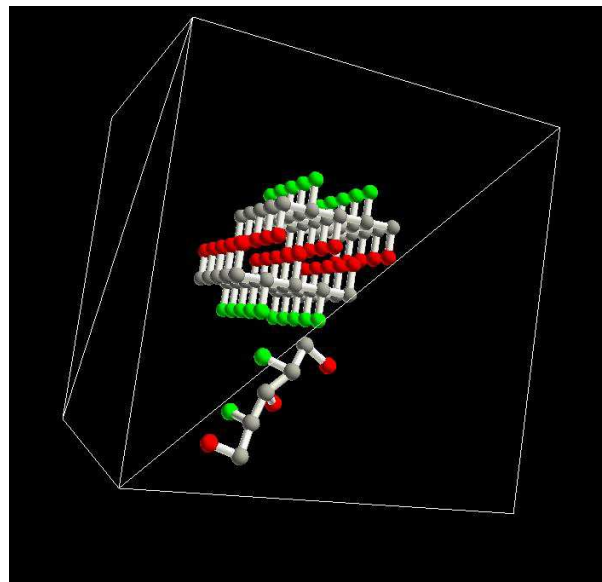
Simulations are done with one fibril segment and one monomer in a cubic box 6 nm on a side (therefore, the monomer concentration  $[m]$  and fibril concentration  $[f]$  is 7.7 mM). A fibril segment consisting of ten 5-amino-acid peptides are placed at the center of the box. The fibril is constructed by hand and consists of two-layer of cross-beta sheet structure as depicted in Fig. 4. The fibril is held fixed, i.e., the peptides within it are completely frozen throughout the simulation. At time zero, a monomeric peptide is placed at the corner of the box and the simulation is stopped when the free monomer has all of the five *D*-bonds formed with the fibril. Note that there are four possible locations for the added monomer to bind to as the fibril has two ends and there are two cross-beta sheets.

Throughout the run, we record the time when a change in the number of *D*-bonds between the monomeric peptide and the fibril happens. This allows us to construct a

TABLE II: A comparison between the parameters employed in the simulations measure (middle column) and the corresponding values measured experimentally (right column). Note that the hydrophobic strength and the hydrogen bond strength in the middle column depicts the enthalpies defined in the simulations while the values in the right columns are measured in free energies. We note that the qualitative nature of our conclusion stays the same when the hydrophobic strength (hydrogen bond strength) are varied around the presented values by twenty (ten) percents above and below.

Properties	Simul.	Exp'l
Friction coefficient per bead, $\gamma$ ( $k_B T \text{ps}/\text{nm}^2$ )	1000	$\sim 1000$ [27]
Inter-amino-acid distance (nm)	0.5	0.35 [28]
Hydrophobic interaction strength ( $k_B T$ )	1.5	1-4 [16]
Hydrogen bond strength ( $k_B T$ )	4	$\sim 2.3$ [16]
Time increment, $\Delta t$ (fs)	5.6	–

FIG. 4: A snapshot of one simulation run in progress. The fibril is put in the middle of the simulation box and the monomer is diffusing towards it. The fibrillar axis is along the  $z$ -axis, the cross-beta sheets are along the  $x$ -axis, and the coordinates of the  $A_3$  bead for the peptides are  $(-0.25, 0.6, k/2 - 1)$  and  $(0.25, 0.6, k/2 - 1.25)$ ,  $k = 0, \dots, 4$ . The corners of the simulation box are at  $x, y, z = \pm 3$ .



time series describing the temporal evolution of the elongation process. We will now describe how the time series is analyzed.

### III. DATA ANALYSIS

To comprehend our simulation results, we adopt a coarse-grained picture of the dynamics of fibril elongation. Specifically, we partition the phase space of a monomer in the process of fibrilization into a number of discrete states, and aim to approximate the dynamical picture by a series of jumps between neighboring states by Markovian processes. The desire to have a Markovian representation is an attempt to view the dynamics through a familiar mechanism. To find a sensible definition for the set of discrete states, we firstly simplify the dynamical picture by recoding the time whenever a  $D$ -bond is formed or destroyed. This gives an array consisting of the times and the numbers of  $D$ -bonds between the monomer and the fibril as shown in Fig. 5(a). By inspection of the dataset, it is apparent that the time series consists of segments of long periods within which there are a lot of rapid back and forth transitions between having  $k$  and  $k + 1$   $D$ -bonds. This is a clear sign of temporal correlation and since our desire is to approximate the process with a memoryless kinetic mechanism, we will partition the configuration space of our system into five discrete states designated by:  $S_0$ ,  $S_{1\leftrightarrow 2}$ ,  $S_{2\leftrightarrow 3}$ ,  $S_{3\leftrightarrow 4}$  and  $S_5$ , where  $S_0$  refers to having no  $A$ -bonds between the monomer and the fibril,  $S_{k\leftrightarrow k+1}$  refers to the state where the number of  $D$ -bonds flickers between  $k$  and  $k + 1$ , and  $S_5$  refers to the fully aligned state for the monomer. With these newly defined states, a new time series recording the transitions between them can be constructed (c.f. Fig. 5 and Fig. 6). We now assume that all the transition events are drawn from Independent and Exponential Distributions. Given the property that the minimum of two exponential random variables is again exponentially distributed with rate equal to the sum of the two original rates, we are able to decouple the individual rate for each transition event from the time series (c.f. footnote 42). The results are shown in Fig. 7.

### IV. DISCUSSION

The diffusion constant of a monomer in our simulations is measured to be  $1.1 \times 10^{-4}$  nm<sup>2</sup>/ps (plots not shown). Since the combined binding area for the monomer and fibril's ends is about 5 nm<sup>2</sup>, we expect that the collision frequency in our system (with  $[m] = [f] = 7.7$  mM) to be about  $5 \times 10^{-5}$  ps<sup>-1</sup>. This is comparable with the rate of transition from state  $S_0$  to state  $S_{1\leftrightarrow 2}$  observed in our simulations (c.f. Fig. 7), we therefore conclude that the initial binding event is well described by a diffusion controlled reaction. We also note that the initial dissociation rate (from state  $S_{1\leftrightarrow 2}$  to state  $S_0$ ) is determined to be  $4.3 \times 10^{-5}$  ps<sup>-1</sup>, which is comparable to our estimate for  $a_-$  in Eq. (2).

Besides the transition rate between  $S_0$  and  $S_{1\leftrightarrow 2}$ , we can see that many of the forward transition rates are of the same order of magnitude as the first binding rate.

FIG. 5: A segment of the data from the simulations. (a) The original time series consists of the times when the number of  $D$ -bond is changed. This is then transformed into a time series on the transitions of the set of states  $\{S\}$  (b). The procedure of transformation is described in the text.

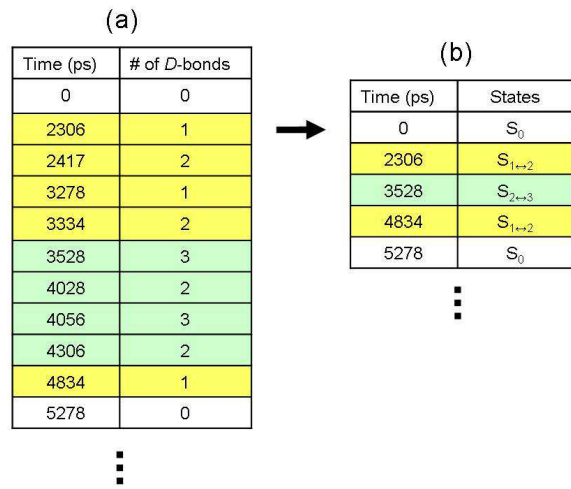


FIG. 6: The numbers of transitions within the set of states  $\{S\}$ . Note the  $ij$ -entry denotes the number of transitions from state  $S_{i-1}$  to  $S_{i-1\leftrightarrow j}$ .

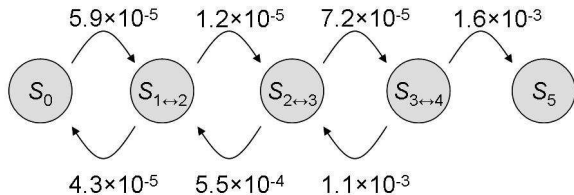
$$\begin{bmatrix} 0 & 751 & 72 & 0 & 0 \\ 4169 & 0 & 1181 & 14 & 0 \\ 0 & 1116 & 0 & 147 & 0 \\ 0 & 4 & 69 & 0 & 100 \end{bmatrix}$$

This demonstrates that the elongation process is not first-order, but rather dominated by frustrations for the monomer to find the correct configuration to become fully part of the fibril, i.e., state  $S_5$  (c.f. Fig. 1). We note that this qualitative picture stays the same when the hydrophobic strength (hydrogen bond strength) are varied around the presented values by twenty (ten) percents above and below. This is the main result of this work.

To have a conceptual feeling for how a rugged energy landscape picture would affect the elongation process, we look at the work by Zwanzig [30], which demonstrates that: if a particle is diffusing over a 1D rugged landscape such that the fluctuation in potential energy is Gaussian distributed with zero mean and standard deviation  $\epsilon$ , then the motion of the particle can be effectively described by ordinary diffusion with a re-defined diffusion constant,  $D^*$ , of the form:

$$D^* = D \exp[-(\epsilon/k_B T)^2] \quad (7)$$

FIG. 7: The transition rates for the set of states  $\{S\}$  constructed from the time series as described in the text. The units are in  $\text{ps}^{-1}$ .



where  $D$  is the original diffusion coefficient.

Let us now consider the elongation process as a drift-diffusion process on a rugged energy landscape (c.f. Fig. 8). Adopting the idea of Zwanzig mentioned above [30], we account the ruggedness by redefining the diffusion constant as in Eq. (7). In other words, the probability distribution,  $p(x, t)$ , of the state of the system (represented by the reaction coordinate  $x$ ) follows the differential equation below:

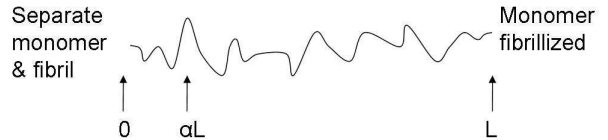
$$\partial_t p(x, t) = D \partial_x^2 p(x, t) - v \partial_x p(x, t). \quad (8)$$

where  $D$  is the renormalized diffusion constant that takes the ruggedness into account, and  $v$  is the drift produced by the free energy descent that drives the monomer to become fibrilized. The differential equation is supplemented by the boundary condition  $p(0, t) = p(L, t) = 0$  where the left boundary depicts monomer detachment from the fibril's end and the right boundary depicts completion of the fibrilization process (c.f. Fig. 8). We will now assume that the initial condition is a delta function located at  $\alpha L$ , i.e.,  $p(x, t = 0) = \delta(x - \alpha L)$ , such that  $\alpha$  is small. If  $v$  is negligible, i.e., when the free energy drive for fibrilization is negligible, the ratio of monomers exiting at the left boundary (becoming detached) and exiting at the right boundary (becoming fibrilized) is proportional to  $\alpha$  [31]. Using the number of hydrogen bonds again as a very crude estimate for the reaction coordinate. For the case A $\beta$  peptides, the total number of hydrogen bonds is likely to be in the order of 20 [32] so if we take the initial location as having one hydrogen bond formed with the fibril,  $\alpha \sim 1/20$ . In other words, according to this diffusion-on-rugged-landscape model, only about 20 monomers would be recycled before one of them is fibrilized, as compared to the  $10^7$  monomers predicted by the two-step model depicted in Eq. (1).

Our models also provides the following experimentally relevant insights on the elongation process:

1. During the period of conversion, the monomer will go through a lot of different conformations, and there is not a specific conformation that acts as the typical conformation before fibrilization.
2. Since the conversion step is slow, the interac-

FIG. 8: A schematic diagram depicting the scenario where the elongation process is viewed as a diffusion process over a rugged energy landscape in 1D. The linear dimension denotes the 'reaction coordinate' and the position  $x_0$  indicates the location when the monomer is first bound to the fibril's end.



tions between multiple monomers at the fibrils' ends should be important, and this propensity for monomers' interactions may also serve to promote oligomers formation. One would also expect that multi-monomer interactions would induce more ruggedness into the landscape picture.

3. Since elongation rates are determined by the form of the energy traps, it is expected that the more uniform the amyloid-forming peptide's sequence is, the slower the elongation rate. This is because primary sequence with many identical side chains would promote misalignment binding and as a result, enhance the ruggedness of the energy landscape. In other words, the complexity of the primary sequence may serve as a factor in elongation rate prediction (c.f. [33, 34, 35, 36, 37, 38]).

## V. CONCLUSION

We have studied the elongation process of amyloid fibril by performing Langevin simulations on a toy model of peptides. By projecting the elongation process onto a set of discrete states, a rugged energy landscape picture emerged, which indicates that monomer-fibril interaction is prolonged in the course of elongation. A crude estimate based on this scheme indicates that in the orders of tens of monomers would have interacted with the end of the fibril before a new monomer is fibrilised. Our findings also suggest that the complexity of an amyloid forming peptide, as measured for instance by how diverse the amino-acid compositions are, may serve as a predictor of the fibril elongation rate. These conclusions can be tested with current experimental techniques.

## Acknowledgments

The simulations are performed with Nereus System [39], a distributive grid computing system developed in Particle Physics (Oxford). CFL thanks the Glasstone

Trust (Oxford) and Jesus College (Oxford), JL the John Fell Oxford University Press Fund, for financial support.

LJ and DJV acknowledge the generous support of Synatica Ltd, a spin-out company of Oxford University.

- 
- [1] M. Sunde, L. C. Serpella, M. Bartlama, P. E. Fräsera, M. B. Pepysa, and C. C. F. Blakea, *Journal of Molecular Biology* **273**, 729 (1997).
- [2] C. M. Dobson, *Nature* **426**, 884 (2003).
- [3] S. Radford, *Trends in Biochemical Sciences* **25**, 611 (2000).
- [4] M. R. Sawaya, S. Sambashivan, R. Nelson, M. I. Ivanova, S. A. Sievers, M. I. Apostol, M. J. Thompson, M. Balbirnie, J. J. W. Wiltzius, H. T. McFarlane, et al., *Nature* **447**, 453 (2007).
- [5] J. D. Harper and P. T. Lansbury, *Annual Review of Biochemistry* **66**, 385 (1997).
- [6] D. Hall, N. Hirota, and C. Dobson, *Journal of Molecular Biology* **351**, 195 (2005).
- [7] Y. Kusumoto, A. Lomakin, D. B. Teplow, and G. B. Benedek, *Proceedings of the National Academy of Sciences of the United States of America* **95**, 12277 (1998).
- [8] W. P. Esler, E. R. Stimson, J. M. Jennings, H. V. Vinters, J. R. Ghilardi, J. P. Lee, P. W. Mantyh, and J. E. Maggio, *Biochemistry* **39**, 6288 (2000).
- [9] F. Massi and J. E. Straub, *Proteins: Structure, Function, and Genetics* **42**, 217 (2001).
- [10] T. Scheibel, J. Bloom, and S. L. Lindquist, *Proceedings of the National Academy of Sciences of the United States of America* **101**, 2287 (2004).
- [11] P. H. Nguyen, M. S. Li, G. Stock, J. E. Straub, and D. Thirumalai, *Proceedings of the National Academy of Sciences* **104**, 111 (2007).
- [12] S. R. Collins, A. Douglass, R. D. Vale, and J. S. Weissman, *PLoS Biology* **2**, e321 (2004).
- [13] A. Lomakin, D. B. Teplow, D. A. Kirschner, and G. B. Benedek, *Proceedings of the National Academy of Sciences of the United States of America* **94**, 7942 (1997).
- [14] T. Ban, M. Hoshino, S. Takahashi, D. Hamada, K. Hasegawa, H. Naiki, and Y. Goto, *Journal of Molecular Biology* **344**, 757 (2004).
- [15] K. Sneppen and G. Zocchi, *Physics in Molecular Biology* (Cambridge University Press, Cambridge, 2005).
- [16] M. B. Jackson, *Molecular and Cellular Biophysics* (Cambridge University Press, Cambridge, 2006).
- [17] C. Monthus and J.-P. Bouchaud, *Journal of Physics A: Mathematical and General* **29**, 3847 (1996).
- [18] S. Peng, F. Ding, B. Urbanc, S. V. Buldyrev, L. Cruz, H. E. Stanley, and N. V. Dokholyan, *Physical Review E (Statistical, Nonlinear, and Soft Matter Physics)* **69**, 041908 (2004).
- [19] H. D. Nguyen and C. K. Hall, *Proceedings of the National Academy of Sciences of the United States of America* **101**, 16180 (2004).
- [20] S. Santini, N. Mousseau, and P. Derreumaux, *J. Am. Chem. Soc.* **126**, 11509 (2004).
- [21] B. Urbanc, L. Cruz, S. Yun, S. V. Buldyrev, G. Bitan, D. B. Teplow, and H. E. Stanley, *Proceedings of the National Academy of Sciences* **101**, 17345 (2004).
- [22] G. Favrin, A. Irback, and S. Mohanty, *Biophys. J.* **87**, 3657 (2004).
- [23] R. Pellarin and A. Caffisch, *Journal of Molecular Biology* **360**, 882 (2006).
- [24] N. Fawzi, Y. Okabe, E. Yap, and T. Headgordon, *Journal of Molecular Biology* **365**, 535 (2007).
- [25] M. S. Li, D. K. Klimov, J. E. Straub, and D. Thirumalai, *The Journal of Chemical Physics* **129**, 175101 (2008).
- [26] C. F. Lee, E-print: arXiv:0802.1985.
- [27] Skjæveland and K. Sneppen, *The European Physical Journal E - Soft Matter* **2**, 285 (2000).
- [28] M. Daune, *Molecular Biophysics: Structures in Motion* (Oxford University Press, Oxford, 1999).
- [29] J. Thijssen, *Computational Physics* (Cambridge University Press, Cambridge, 2007), 2nd ed.
- [30] R. Zwanzig, *Proceedings of the National Academy of Sciences of the United States of America* **85**, 2029 (1988).
- [31] Z. Farkas and T. Fülöp, *Journal of Physics A: Mathematical and General* **34**, 3191 (2001).
- [32] A. T. Petkova, Y. Ishii, J. J. Balbach, O. N. Antzutkin, R. D. Leapman, F. Delaglio, and R. Tycko, *Proceedings of the National Academy of Sciences* **99**, 16742 (2002).
- [33] S. Yoon and W. J. Welsh, *Protein Science* **13**, 2149 (2004).
- [34] A. M. Fernandez-Escamilla, F. Rousseau, J. Schymkowitz, and L. Serrano, *Nature Biotechnology* **22**, 1302 (2004).
- [35] G. G. Tartaglia, A. Cavalli, R. Pellarin, and A. Caffisch, *Protein Science* **14**, 2723 (2005).
- [36] O. V. Galzitskaya, S. O. Garbuzynskiy, and M. Y. Lobanov, *PLoS Computational Biology* **2**, e177 (2006).
- [37] K. F. Dubay, A. P. Pawar, F. Chiti, J. Zurdo, C. M. Dobson, and M. Vendruscolo, *Journal of Molecular Biology* **341**, 1317 (2004).
- [38] A. Pawar, K. Dubay, J. Zurdo, F. Chiti, M. Vendruscolo, and C. Dobson, *Journal of Molecular Biology* **350**, 379 (2005).
- [39] Nereus, <http://www-nereus.physics.ox.ac.uk/> (2008).
- [40] This estimation comes from the property that the minimum of two variables drawn from two independent exponential distributions with rates  $\lambda_1$  and  $\lambda_2$  is again exponentially distributed with rates  $\lambda_1 + \lambda_2$ , and that the probability of having the minimum drawn from the first distribution is  $\lambda_1/(\lambda_1 + \lambda_2)$ .